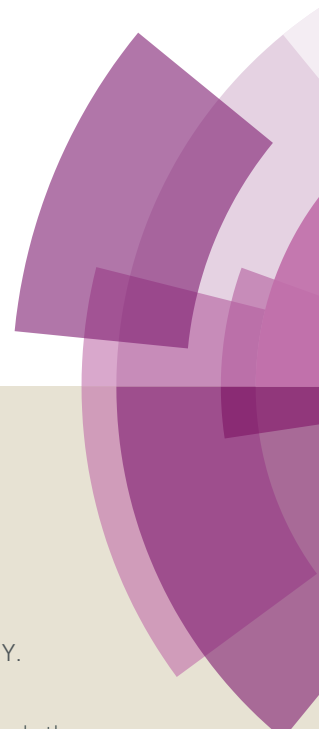


Journal of Materials Chemistry C

Accepted Manuscript



This article can be cited before page numbers have been issued, to do this please use: J. Ding, Z. Yan, Y. Wang, Y. Wang and L. Wang, *J. Mater. Chem. C*, 2017, DOI: 10.1039/C7TC04269H.



This is an Accepted Manuscript, which has been through the Royal Society of Chemistry peer review process and has been accepted for publication.

Accepted Manuscripts are published online shortly after acceptance, before technical editing, formatting and proof reading. Using this free service, authors can make their results available to the community, in citable form, before we publish the edited article. We will replace this Accepted Manuscript with the edited and formatted Advance Article as soon as it is available.

You can find more information about Accepted Manuscripts in the [author guidelines](#).

Please note that technical editing may introduce minor changes to the text and/or graphics, which may alter content. The journal's standard [Terms & Conditions](#) and the ethical guidelines, outlined in our [author and reviewer resource centre](#), still apply. In no event shall the Royal Society of Chemistry be held responsible for any errors or omissions in this Accepted Manuscript or any consequences arising from the use of any information it contains.



Journal Name

ARTICLE

Methoxyl modification in furo[3,2-c]pyridine based iridium complexes towards highly efficient green- and orange-emitting electrophosphorescent devices

Zhimin Yan,^{a,b} Yanping Wang,^c Junqiao Ding,^{*b} Yue Wang,^{*a} Lixiang Wang^{*b}

Received 00th January 20xx,
Accepted 00th January 20xx

DOI: 10.1039/x0xx00000x

www.rsc.org/

Two new furo[3,2-c]pyridine based Ir complexes, namely (4-MeOpfupy)₂Ir(acac) and (3-MeOpfupy)₂Ir(acac), have been designed and synthesized by introducing methoxyl into the 4- and 3-position of phenyl ring on the C^N ligand. It is found that the position of methoxyl plays an important role on the electrochemical and photophysical properties as well as electrophosphorescent device performance. Compared to the reference complex (pfupy)₂Ir(acac) without any methoxyl (538 nm), (4-MeOpfupy)₂Ir(acac) with 4-position methoxyl shows a blue-shifted emission peaked at 523 nm originating from the methoxyl-induced enhancement of the LUMO level, whereas (3-MeOpfupy)₂Ir(acac) with 3-position methoxyl shows a red-shifted emission peaked at 602 nm originating from the methoxyl-induced enhancement of the HOMO level. The corresponding PhOLEDs based on (4-MeOpfupy)₂Ir(acac) and (3-MeOpfupy)₂Ir(acac) realize highly efficient green and orange electroluminescence with CIE coordinates of (0.37, 0.60) and (0.60, 0.40), revealing a state-of-art EQE as high as 29.5% (100.7 cd/A) and 16.7% (43.9 cd/A), respectively. The impressive results indicate that methoxyl modification is a valid way to tune the molecular energy levels and emissive color for Ir complexes while not obviously sacrificing the final device performance.

Introduction

Alkoxy is one of the basic substituents in organic chemistry owing to its facile synthesis through a Williamson route.¹⁻⁴ Unlike the other groups (e.g. alkyl, amine, halogen, cyano and nitro), it displays two opposite electronic effect: 1) a resonance electron-donating effect due to the lone pair electrons of oxygen; 2) an inductive electron-withdrawing effect due to the stronger electronegativity of oxygen than carbon.^{5, 6} Since the resonance electron-donating effect is dominant over the inductive electron-withdrawing one, alkoxy is often seen as an electron-donating group.⁷ Therefore, it could be purposely used to modulate the molecular energy level at the same time when introduced to the conjugated main chain to increase the solubility of conjugated polymers.⁸⁻⁹ For instance, in

quinoxaline based polymers PTTQx, the meta-alkoxy-phenyl was found to reduce the highest occupied molecular orbital (HOMO) level and lowest unoccupied molecular orbital (LUMO) level with respect to the para-alkoxy-phenyl.¹⁰ Further replacing alkylthienyl with meta-alkoxy-phenyl in benzo[1,2-b;4,5-b]dithiophene (BDT) based two-dimensional conjugated polymers led to the significant enhancement of the open-circuit voltage from 0.60 V to 0.78 V and consequently improved power conversion efficiency from 5.56% to 7.50% for the corresponding polymer solar cells (PSCs).¹¹ On the other hand, the emission color regulation of iridium (Ir) complexes, which is related to their energy levels, is also a research hotspot in phosphorescent organic light-emitting diodes (PhOLEDs).¹²⁻²⁹ Although alkoxy was incorporated into Ir complexes, few systematic investigations have been reported about the effect of alkoxy on their photophysical properties and final device performance.³⁰⁻³³

In previous work, we designed and synthesized a novel furo[3,2-c]pyridine based Ir complex (pfupy)₂Ir(acac)³⁴ by replacing sulfur with oxygen in the C^N ligand. Compared with the typical thiophene-containing yellow phosphor (pthpy)₂Ir(acac), a hypsochromic shift was observed for the furan-containing (pfupy)₂Ir(acac), which exhibits a yellowish-green emission with Commission International De L'Eclairage (CIE) coordinates of (0.44, 0.55) and an unexpected external quantum efficiency (EQE) over 30% without any out-coupling technology. Considering the deviated emission of (pfupy)₂Ir(acac) from the green region, there will be

^a State Key Laboratory of Supramolecular Structure and Materials
College of Chemistry, Jilin University
Changchun, 130012, P. R. China
*E-mail: yuewang@jlu.edu.cn

^b State Key Laboratory of Polymer Physics and Chemistry
Changchun Institute of Applied Chemistry, Chinese Academy of Sciences
Changchun, 130022, P. R. China
*E-mail: junqiaod@ciac.ac.cn, lixiang@ciac.ac.cn

^c School of Materials Science and Engineering
Changchun University of Science and Technology
Changchun 130022, P. R. China

Electronic Supplementary Information (ESI) available: ¹H NMR and MALDI-TOF mass spectrometry, crystal details and packing diagrams, TGA, transient PL spectra, CCDC number: 1551044. See DOI: 10.1039/x0xx00000x

ARTICLE

Journal Name

plenty of room for improvements in color purity while not sacrificing device efficiency.

With this idea in mind, we further demonstrate the methoxyl modification in (pfupy)₂Ir(acac) towards highly efficient green- and orange-emitting PhOLEDs. When the methoxyl locates at the 4-position of phenyl in the C^N ligand, the resultant complex (denoted as (4-MeOpfupy)₂Ir(acac)) achieves a more greenish emission than (pfupy)₂Ir(acac), revealing CIE coordinates of (0.37, 0.60) and a peak EQE of 29.5% (100.7 cd/A). Meanwhile, the 3-position substitution of methoxyl on phenyl can endow the resultant complex (denoted as (3-MeOpfupy)₂Ir(acac)) with a red-shifted orange emission accompanied by CIE coordinates of (0.60, 0.40) and a peak EQE of 16.7% (43.9 cd/A). The impressive results manifest that methoxyl modification is a valid way not only to tune the emissive wavelength of Ir complexes but also to keep the high device efficiency.

Experimental

Measurements and Characterization

¹H NMR spectra were recorded by Bruker Avance NMR spectrometer. The elemental analysis was performed using a Bio-Rad elemental analysis system. MALDI/TOF (Matrix assisted laser desorption ionization/Time-of-flight) mass spectra were performed on an AXIMA CFR MS apparatus (COMPACT) with 2-[(2E)-3-(4-tert-butylphenyl)-2-methylprop-2-enylidene] malononitrile (DCTB) as the matrix. Thermal gravimetric analysis (TGA) and differential scanning calorimetry (DSC) were performed under a flow of nitrogen using a Perkin-Elmer-TGA 7 and Perkin-Elmer-DSC 7 system, respectively. The UV-Vis absorption and photoluminescence (PL) spectra were measured by a Perkin-Elmer Lambda 35 UV/Vis spectrometer and a Perkin-Elmer LS 50B spectrofluorometer, respectively. The PL quantum yields (PLQYs) were measured in N₂-saturated toluene solutions with a typical green phosphor Ir(ppy)₃ (Φ_{PL} = 0.97) as the reference.³⁵ The transient PL spectra in toluene solutions were measured under N₂ atmosphere and excited at a 355 nm pulse with ca. 3 ns width from a Quanta-Ray DCR-2 pulsed Nd:YAG laser. Cyclic voltammetry (CV) experiments were performed on a CHI660a electrochemical analyzer under a scan rate of 100 mV s⁻¹. The measurements were carried out in dichloromethane (DCM) for anodic sweeping and in *N,N*-dimethylformamide (DMF) for cathodic sweeping with a conventional three-electrode system consisting of a platinum working electrode, a platinum counter electrode and an Ag/AgCl reference electrode. The supporting electrolyte was 0.1 M tetrabutylammonium perchlorate (*n*-Bu₄NClO₄). All potentials were calibrated against the ferrocene/ferrocenium couple (Fc/Fc⁺). The HOMO and LUMO energy levels were determined by the equations HOMO = -e(E_{ox, onset} + 4.8 V) and LUMO = -e(E_{red, onset} + 4.8 V), where E_{ox, onset} and E_{red, onset} were the potential onset obtained from the first oxidation and reduction waves, respectively. The theoretical calculations were performed on Gauss 09 program. And the ground state structures of Ir complexes were optimized by the DFT using the B3LYP hybrid functional. The "double-ξ" basis set LANL2DZ was employed for Ir atom and 6-31G(d) basis sets for H, C, N, and O atoms.

Synthesis

All chemicals and reagents were used as received from commercial sources without further purification. Solvents for chemical synthesis were purified according to the standard procedures.

General procedure for the synthesis of C^N ligands

To a mixture of 4-chlorofuro[3,2-*c*]pyridine (1 equiv.), methoxyphenyl boronic acid (1.5 equiv.) and Pd(PPh₃)₄ (0.03 equiv.), the refined tetrahydrofuran (THF) and degassed 2M Na₂CO₃ a.q (3 equiv.) were added in an argon atmosphere. After heating to reflux for 8 h, the organic layer was extracted by DCM and dried by Na₂SO₄. The crude product was purified by chromatography on silica gel using petroleum ether and ethyl acetate as the eluent.

4-MeOpfupy: 75% yield. ¹H NMR (400 MHz, CDCl₃) δ 8.66 (dd, *J* = 9.2, 6.0 Hz, 1H), 8.01 (dd, *J* = 11.4, 5.5 Hz, 2H), 7.83 (d, *J* = 12.0 Hz, 1H), 7.53 (dd, *J* = 8.6, 5.1 Hz, 1H), 7.20 – 7.14 (m, 1H), 7.14 (s, 2H), 3.91 (d, *J* = 1.3 Hz, 3H).

3-MeOpfupy: 78% yield. ¹H NMR (400 MHz, CDCl₃) δ 8.68 (d, *J* = 6.0 Hz, 1H), 7.81 (d, *J* = 2.3 Hz, 1H), 7.63 – 7.60 (m, 1H), 7.59 – 7.52 (m, 2H), 7.47 (t, *J* = 7.9 Hz, 1H), 7.17 (dd, *J* = 2.2, 0.9 Hz, 1H), 7.08 (ddd, *J* = 8.2, 2.6, 0.9 Hz, 1H), 3.95 (s, 3H).

General procedure for the synthesis of Ir complexes

IrCl₃•3H₂O (1 equiv.), C^N ligand (2.1 equiv.), 2-ethoxyethanol and H₂O were added to a round bottom flask. The mixture was stirred at 110 °C in argon atmosphere for 48 h. After cooling, the mixture was directly filtered and washed with water and ethanol. The yellow solid (dimer) was dried in vacuum at 65 °C without further purification. Subsequently, a round bottom flask was charged with dimer (1 equiv.), 2,4-pentanedione (5 equiv.) and Na₂CO₃ (5 equiv.). After heated to 80 °C in argon atmosphere for 12 h, the mixture was cooled, and the resulting solid was collected by filtration and washed with water. Further purification was operated by column chromatography using DCM and petroleum ether as the eluent.

(4-MeOpfupy)₂Ir(acac): 61% yield. ¹H NMR (400 MHz, DMSO) δ 8.34 (d, *J* = 2.3 Hz, 2H), 8.26 (d, *J* = 6.6 Hz, 2H), 8.01 (d, *J* = 8.7 Hz, 2H), 7.88 (d, *J* = 1.7 Hz, 2H), 7.67 (dd, *J* = 6.6, 0.7 Hz, 2H), 6.46 (dd, *J* = 8.7, 2.6 Hz, 2H), 5.48 (d, *J* = 2.6 Hz, 2H), 5.26 (s, 1H), 3.44 (s, 6H), 1.70 (s, 6H). MALDI-TOF MS: 740.1 [M⁺]. Anal. calcd for C₃₃H₂₇IrN₂O₆: C, 53.58; H, 3.68; N, 3.79. Found: C, 53.30; H, 3.65; N, 3.70.

(3-MeOpfupy)₂Ir(acac): 35% yield. ¹H NMR (400 MHz, DMSO) δ 8.37 (d, *J* = 2.3 Hz, 2H), 8.33 (d, *J* = 6.5 Hz, 2H), 7.87 (d, *J* = 1.7 Hz, 2H), 7.75 (d, *J* = 6.5 Hz, 2H), 7.53 (d, *J* = 2.6 Hz, 2H), 6.36 (dd, *J* = 8.4, 2.6 Hz, 2H), 5.91 (d, *J* = 8.4 Hz, 2H), 5.25 (s, 1H), 3.71 (s, 6H), 1.69 (s,

6H). MALDI-TOF MS: 740.1 [M⁺]. Anal. calcd for C₃₃H₂₇IrN₂O₆: C, 53.58; H, 3.68; N, 3.79. Found: C, 52.99; H, 3.63; N, 3.67.

Device fabrication and testing

All the devices were fabricated on glass substrates pre-coated with 180 nm indium tin oxide (ITO) with a sheet resistance of 10 Ω/sq. The ITO substrates were degreased in ultrasonic solvent bath and then dried at 120 °C for 30 min. Before loaded into the vacuum deposition chamber, the ITO surface was treated with UV-ozone for 15 min. In successive, 10 nm of MoO₃ was deposited on the top of ITO, followed by 60 nm TAPC (4,4'-(cyclohexane-1,1-diyl)bis(N,N-dip-tolylaniline)), 5 nm TCTA (tris(4-(9H-carbazol-9-yl)phenyl)amine), 20 nm emissive layer, and 35 nm BmPyPB (3,3'',5,5''-tetra(pyridin-3-yl)-1,1':3',1''-terphenyl). Finally, 1 nm thickness of LiF and 120 nm thickness of Al were deposited to form the cathode. All the layers were grown by thermal evaporation in a high-vacuum system with a pressure of less than 5×10⁻⁴ Pa without breaking vacuum. The organic materials were evaporated at the rate in a range of 1-2 Å/s while the evaporation rate of LiF layer is 0.1 Å/s, and the metal Al was evaporated at a rate of 8-10 Å/s. The overlap between ITO and Al electrodes was 4 mm × 4 mm, which is the active emissive area of PhOLEDs. The current-voltage-brightness characteristics were measured by using a set of Keithley source measurement units (Keithley 2400 and Keithley 2000) with a calibrated silicon photodiode. The electroluminescence (EL) spectra were measured by a Spectrascan PR650 spectrophotometer. All the measurements were carried out in ambient atmosphere at room temperature.

X-ray Crystallography Analysis

The single crystal X-ray diffraction experiments were carried out using a Bruker Smart APEX diffractometer with CCD detector and graphite monochromator, Mo Kα radiation (λ = 0.71073 Å). The intensity data were recorded with ω scan mode (187 K). Lorentz, polarization factors were made for the intensity data and absorption corrections were performed using SADABS program. The crystal structure was determined using the SHELXTL program and

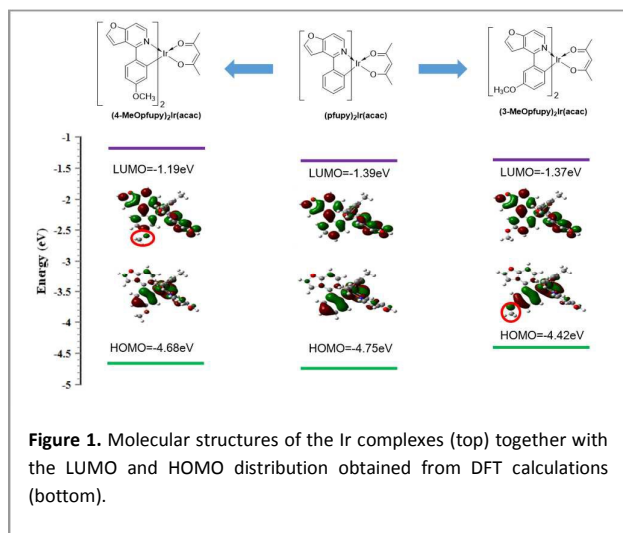
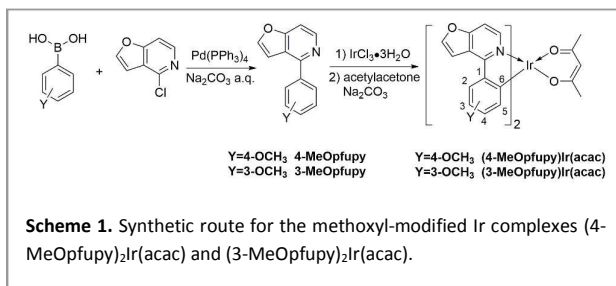


Figure 1. Molecular structures of the Ir complexes (top) together with the LUMO and HOMO distribution obtained from DFT calculations (bottom).



Scheme 1. Synthetic route for the methoxyl-modified Ir complexes (4-MeOpfupy)₂Ir(acac) and (3-MeOpfupy)₂Ir(acac).

refined using full matrix least squares. All non-hydrogen atoms were assigned with anisotropic displacement parameters, whereas hydrogen atoms were placed at calculated positions theoretically and included in the final cycles of refinement in a riding model along with the attached carbons.

Results and discussion

Molecular design, synthesis and characterization

Starting from (pfupy)₂Ir(acac), methoxyl is introduced to the 4- and 3-positions of phenyl to design the corresponding Ir complexes (4-MeOpfupy)₂Ir(acac) and (3-MeOpfupy)₂Ir(acac), respectively. As depicted in Figure 1, the LUMO is mainly localized on furo[3,2-c]pyridine and phenyl, while the HOMO is concentrated on Ir centre and phenyl in (pfupy)₂Ir(acac). And varying the methoxyl positions on (pfupy)₂Ir(acac) can lead to the different LUMO and HOMO

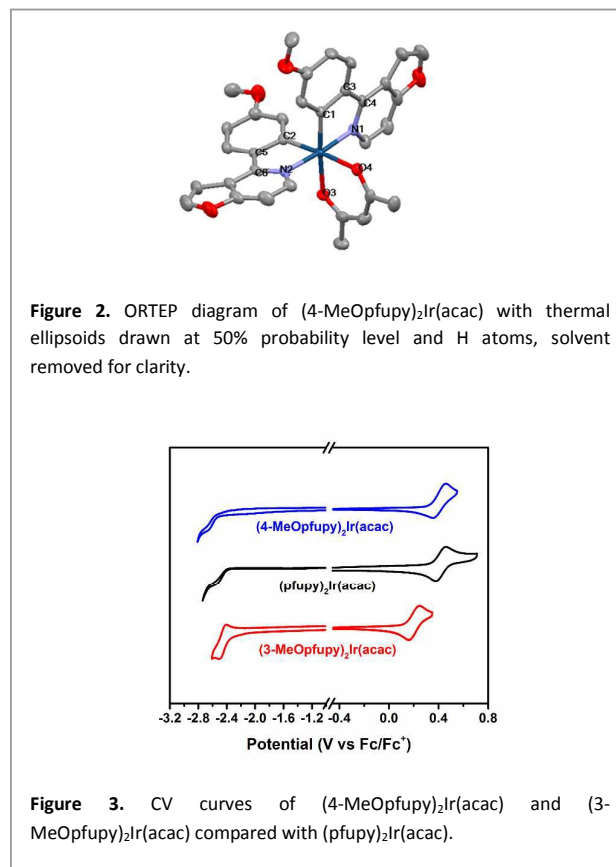


Figure 2. ORTEP diagram of (4-MeOpfupy)₂Ir(acac) with thermal ellipsoids drawn at 50% probability level and H atoms, solvent removed for clarity.

Figure 3. CV curves of (4-MeOpfupy)₂Ir(acac) and (3-MeOpfupy)₂Ir(acac) compared with (pfupy)₂Ir(acac).

distribution. For example, in (4-MeOpfupy)₂Ir(acac) where the methoxyl group is meta to Ir centre but para to furo[3,2-c]pyridine, its contribution to furo[3,2-c]pyridine by the resonance electron-donating effect is stronger than that to Ir centre. Accordingly, the LUMO distribution of (4-MeOpfupy)₂Ir(acac) is extended to methoxyl without obviously affecting the HOMO one. Benefiting from the elevated LUMO and similar HOMO energy levels, a wide bandgap could be anticipated for (4-MeOpfupy)₂Ir(acac) relative to (pfupy)₂Ir(acac). By contrast, in (3-MeOpfupy)₂Ir(acac), the methoxyl group does contribute to the HOMO distribution rather than the LUMO one because of the para arrangement between methoxyl and Ir centre. From (pfupy)₂Ir(acac) to (3-MeOpfupy)₂Ir(acac), therefore, the HOMO energy level is increased and the LUMO remains nearly unchanged, resulting in a shallow bandgap. The DFT calculations clearly indicate the effectiveness of methoxyl to modulate the molecular energy levels of furo[3,2-c]pyridine based Ir complexes.

The synthetic procedure for (4-MeOpfupy)₂Ir(acac) and (3-MeOpfupy)₂Ir(acac) is shown in Scheme 1. The furo[3,2-c]pyridine based C^N ligands were firstly prepared by a Suzuki coupling reaction between 4-chlorofuro[3,2-c]pyridine and corresponding methoxyl-functionalized boric acids. Then a traditional two step route was performed to afford the terminal Ir complexes as reported by M. E. Thompson.³⁶ Their molecular structures were fully characterized by ¹H NMR spectroscopy, MALDI-TOF mass spectrometry and elemental analysis (Figure S1-S2). In addition, the single crystal of (4-MeOpfupy)₂Ir(acac) for X-ray diffraction analysis was successfully grown from the mixed solution of DCM and methanol, but the attempt to the single crystal of (3-MeOpfupy)₂Ir(acac) failed. As one can see in Figure 2, (4-MeOpfupy)₂Ir(acac) assumes a similar distorted quasi-octahedral geometric structure to (pfupy)₂Ir(acac).³⁴ Nevertheless, different from (pfupy)₂Ir(acac) showing a π-π interaction between furo[3,2-c]pyridine and phenyl ring, an interaction between two furo[3,2-c]pyridine moieties with a π-π stacking distance of 3.267-3.287 Å is actually observed for (4-MeOpfupy)₂Ir(acac) (Figure S3). The difference may be tentatively attributed to the steric hindrance from methoxyl substituted on phenyl.

Electrochemical properties

CV was used to study the electrochemical properties of (4-MeOpfupy)₂Ir(acac) and (3-MeOpfupy)₂Ir(acac) relative to

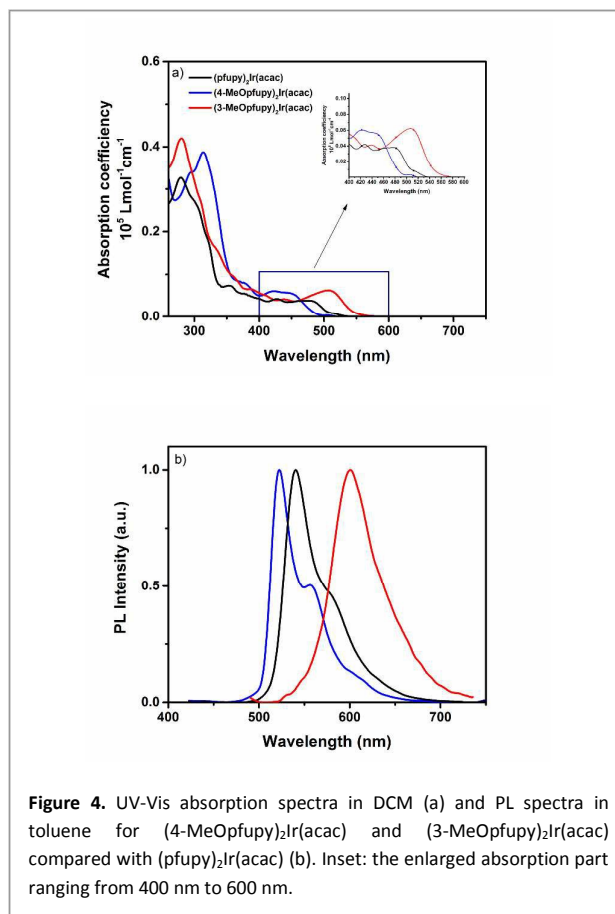


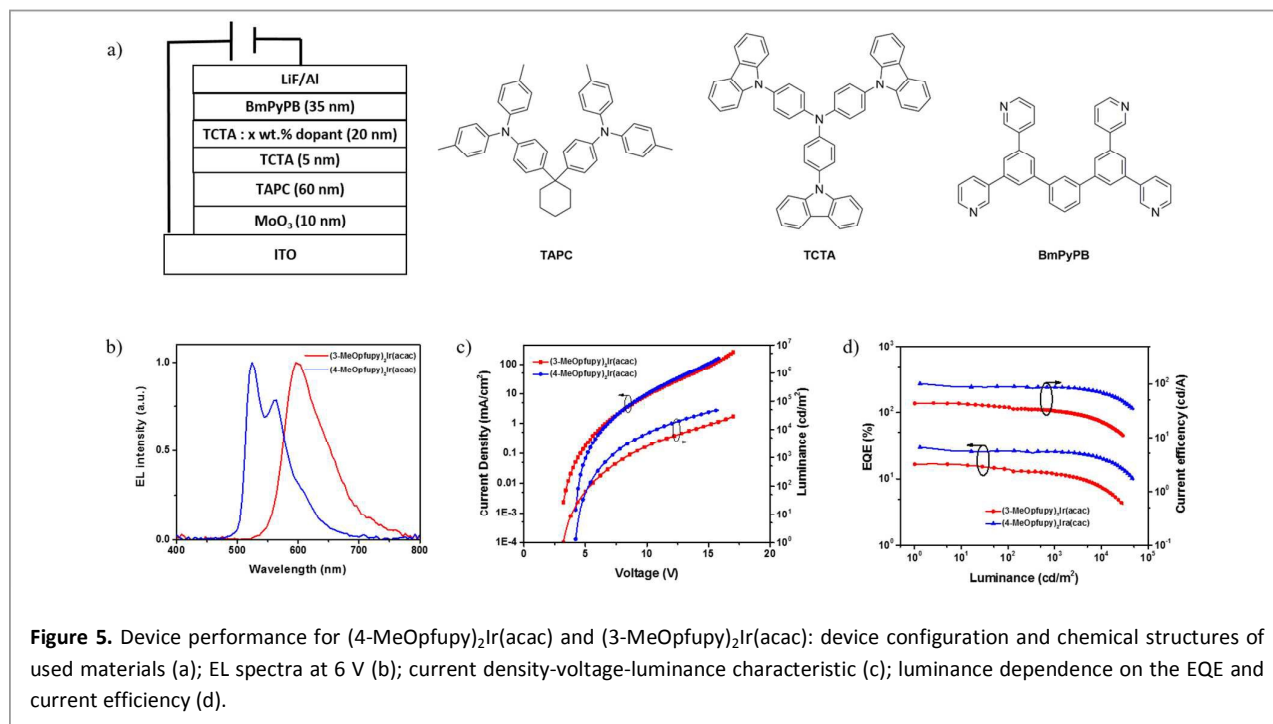
Figure 4. UV-Vis absorption spectra in DCM (a) and PL spectra in toluene for (4-MeOpfupy)₂Ir(acac) and (3-MeOpfupy)₂Ir(acac) compared with (pfupy)₂Ir(acac) (b). Inset: the enlarged absorption part ranging from 400 nm to 600 nm.

(pfupy)₂Ir(acac). For all the Ir complexes, a reversible oxidation and an irreversible reduction are detected during the anodic scan in DCM and cathodic scan in DMF, respectively (Figure 3). With respect to Fc/Fc⁺ (4.8 eV under vacuum), their corresponding HOMO and LUMO levels can be determined, and the data are tabulated in Table 1. Compared with (pfupy)₂Ir(acac) (HOMO: -5.15 eV; LUMO: -2.40 eV), (4-MeOpfupy)₂Ir(acac) displays an invariable HOMO of -5.15 eV and an elevated LUMO of -2.29 eV, whereas (3-MeOpfupy)₂Ir(acac) exhibits an enhanced HOMO of -4.94 eV and a close LUMO of -2.45 eV. The experimental trend is in well line with the DFT calculations at the beginning of the molecular design.

Table 1. Photophysical, electrochemical and thermal properties of (4-MeOpfupy)₂Ir(acac) and (3-MeOpfupy)₂Ir(acac) relative to (pfupy)₂Ir(acac).

Complex	λ_{abs}^a [nm]	λ_{em}^b [nm]	Φ_{PL}^c	τ^d [μs]	HOMO ^e [eV]	LUMO ^e [eV]	T_d^f [°C]	k_r^g [s ⁻¹]	k_{nr}^g [s ⁻¹]
(pfupy) ₂ Ir(acac)	279, 355, 426, 479	538	0.80	1.04	-5.15 (-4.75)	-2.40 (-1.39)	354	7.7×10^5	1.9×10^5
(4-MeOpfupy) ₂ Ir(acac)	296, 314, 422, 444	523	0.88	1.07	-5.15 (-4.68)	-2.29 (-1.19)	350	8.2×10^5	1.1×10^5
(3-MeOpfupy) ₂ Ir(acac)	280, 386, 439, 507	602	0.32	1.33	-4.94 (-4.42)	-2.45 (-1.42)	323	2.4×10^5	5.1×10^5

^a Measured in 10⁻⁵ M DCM solution; ^b Measured in 10⁻⁵ M toluene solution; ^c Measured in N₂-saturated toluene solution with Ir(ppy)₃ ($\Phi_{\text{PL}} = 0.97$) as the reference; ^d Estimated from the transient PL spectrum measured in N₂-saturated toluene solution excited by a 355 nm pulse; ^e HOMO = -e($E_{\text{ox, onset}} + 4.8$ V), LUMO = -e($E_{\text{red, onset}} + 4.8$ V), where $E_{\text{ox, onset}}$ and $E_{\text{red, onset}}$ are the onset values of the first oxidation and reduction waves, respectively. The corresponding data from DFT calculations were also shown in brackets; ^f Decomposition temperature corresponding to a 5% weight loss; ^g Calculated according to the equations: $\tau = 1/(k_r + k_{nr})$ and $\Phi = k_r/(k_r + k_{nr})$.



Photophysical properties

Figure 4 portrays the UV-Vis absorption and PL spectra in diluted solutions. Similar to (pfupy)₂Ir(acac), both (4-MeOpfupy)₂Ir(acac) and (3-MeOpfupy)₂Ir(acac) possess two absorption bands including the intense ligand-centered (LC) π - π^* absorption below 400 nm and the weak metal-to-ligand charge transfer (MLCT) absorption in the range of 400-575 nm (Figure 4a).¹³ Moreover, the lowest-energy-level absorption shows an obvious bathochromic shift following a sequence of (4-MeOpfupy)₂Ir(acac), (pfupy)₂Ir(acac) and (3-MeOpfupy)₂Ir(acac). Correspondingly, the emission maxima move from 523 nm to 538 nm and 602 nm (Figure 4b). The methoxyl dependence on the optical properties is consistent with the electrochemical properties as well as the DFT simulations. As discussed above, the blue-shifted absorption and PL of (4-MeOpfupy)₂Ir(acac) could be ascribed to the wider bandgap than (pfupy)₂Ir(acac), originating from the 4-position methoxyl contribution mainly to the increased LUMO level. And for (3-MeOpfupy)₂Ir(acac), the rise of the HOMO level caused by the 3-position methoxyl is responsible for the shallower bandgap, and thus red-shifted absorption and PL with regard to (pfupy)₂Ir(acac).

In comparison to (pfupy)₂Ir(acac) (1.04 μ s), close decay lifetimes

of 1.07 μ s and 1.33 μ s are determined for (4-MeOpfupy)₂Ir(acac) and (3-MeOpfupy)₂Ir(acac), respectively (Figure S4). Despite this, the PLQY of (4-MeOpfupy)₂Ir(acac) (0.88) seems to be a bit higher than that of (pfupy)₂Ir(acac) (0.80) because of the slightly faster radiative rate constant (k_r) and slower non-radiative rate constant (k_{nr}). On the contrary, (3-MeOpfupy)₂Ir(acac) shows a significantly descent PLQY of 0.32 with a tardy k_r and rapid k_{nr} owing to the energy gap law.³⁷

EL properties

To evaluate whether these Ir complexes are suitable for the evaporation deposition method, TGA was performed to detect their decomposition temperatures (T_d) corresponding to a 5% weight loss. It is found that the introduction of methoxyl has little influence on the thermal stability. For example, (4-MeOpfupy)₂Ir(acac) shows an almost equal T_d of 354 °C to (pfupy)₂Ir(acac), and (3-MeOpfupy)₂Ir(acac) exhibits a slightly lower T_d of 323 °C (Figure S5 and Table 1). Such a relative high T_d above 300 °C can ensure the further thermal-deposited device test for (4-MeOpfupy)₂Ir(acac) and (3-MeOpfupy)₂Ir(acac). Moreover, no obvious glass transition behaviours are observed for (4-MeOpfupy)₂Ir(acac) and (3-

Table 2. Device performance for (4-MeOpfupy)₂Ir(acac) and (3-MeOpfupy)₂Ir(acac).

	V_{on}^a [V]	L_{max} [cd/m ²]	η_c^b [cd/A]	η_p^b [lm/W]	EQE ^b [%]	CIE ^c [x, y]
(4-MeOpfupy) ₂ Ir(acac)	4.2	48790	100.7/86.3/76.7	75.3/38.7/25.6	29.5/25.2/22.8	0.37, 0.60
(3-MeOpfupy) ₂ Ir(acac)	3.2	28885	43.9/30.7/24.4	42.5/11.5/6.5	16.7/11.9/9.2	0.60, 0.40

^a Turn-on voltage at a brightness of 1 cd/m²; ^b maximum data, data at 1000 cd/m² and 5000 cd/m² for current efficiency (η_c), power efficiency (η_p) and EQE, respectively; ^c CIE at 1000 cd/m².

ARTICLE

Journal Name

MeOpfupy)₂Ir(acac) in their DSC curves (Inset in Figure S5), meaning the formation of amorphous films during thermal deposition.

Then we utilized them as the triplet dopants to fabricate PhOLEDs with a structure of ITO/MoO₃ (10 nm)/TAPC (60 nm)/TCTA (5 nm)/TCTA: Ir complex (20 nm)/BmPyPB (35 nm)/LiF (1 nm)/Al (100 nm). Here MoO₃ and LiF were used as the hole- and electron-injecting layers, respectively; TAPC and BmPyPB were employed as the hole- and electron-transporting layers, respectively; and TCTA was adopted as the electron-blocking layer and the host at the same time (Figure 5a). The best doping concentration was optimized to be 6 wt.% and 4 wt.% for (4-MeOpfupy)₂Ir(acac) and (3-MeOpfupy)₂Ir(acac), respectively. As can be clearly seen in Figure 5b, (4-MeOpfupy)₂Ir(acac) emits a bright green EL peaked at 524 nm. Compared to the yellowish-green (pfupy)₂Ir(acac) (CIE: (0.44, 0.55)), the CIE coordinates of (4-MeOpfupy)₂Ir(acac) are blue-shifted to (0.37, 0.60) and are more close to the standard viz. (0.30, 0.60) for green light, indicative of the better green color purity. Meanwhile, an orange EL peaked at 597 nm is observed for (3-MeOpfupy)₂Ir(acac), giving CIE coordinates of (0.60, 0.40).

Figure 5c and 5d plot the current density-voltage-luminance characteristics and the luminance dependence on the EQE and current efficiency, respectively. We note that the turn-on voltage at 1 cd/m² of (4-MeOpfupy)₂Ir(acac) is 4.2 V, higher than that of (3-MeOpfupy)₂Ir(acac) (3.2 V). The observation is understandable when considering the large charge injection barrier induced by the wider bandgap of (4-MeOpfupy)₂Ir(acac) relative to (3-MeOpfupy)₂Ir(acac), which is further confirmed by the lower current density at a driving voltage below 6 V. In spite of this, high device performance is achieved for the green-emitting (4-MeOpfupy)₂Ir(acac), revealing a maximum luminance of 48790 cd/m², a peak current efficiency of 100.7 cd/A and a peak EQE of 29.5%. And the orange-emitting (3-MeOpfupy)₂Ir(acac) gives a maximum luminance of 28885 cd/m², a peak current efficiency of 43.9 cd/A and a peak EQE of 16.7%. To our knowledge, the obtained performance is among the best for green³⁸⁻⁴⁰ and orange⁴¹⁻⁴³ PhOLEDs.

Conclusions

In summary, we report two new methoxyl-functionalized Ir complexes bearing furo[3,2-c]pyridine based C^N ligand. By simply modifying the methoxyl position on the ligand, highly efficient green- and orange-emitting PhOLEDs can be realized at the same time. Compared to (pfupy)₂Ir(acac) without any methoxyl, (4-MeOpfupy)₂Ir(acac) with 4-position methoxyl shows a blue-shifted green emission of 523 nm accompanied by CIE coordinates of (0.37, 0.60) and a peak EQE of 29.5%, while (3-MeOpfupy)₂Ir(acac) with 3-position methoxyl shows a red-shifted orange emission of 602 nm accompanied by CIE coordinates of (0.60, 0.40) and a peak EQE of 16.7%. We believe that this work will shed light on the great potential of furo[3,2-c]pyridine based Ir complexes in high-performance PhOLEDs.

Acknowledgements

This work was supported by the National Key Research and Development Program of China (No. 2016YFB0400701) and the National Natural Science Foundation of China (No. 51573183, 91333205 and 21174144).

Conflicts of interest

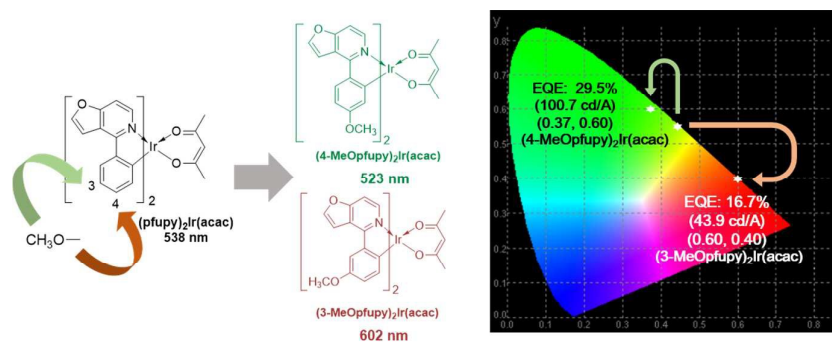
There are no conflicts of interest to declare.

Notes and references

1. A. Williamson, *Philos. Mag.*, 1850, **37**, 350-356.
2. Y. Wang, S. Wang, N. Zhao, B. Gao, S. Shao, J. Ding, L. Wang, X. Jing and F. Wang, *Polym. Chem.*, 2015, **6**, 1180-1191.
3. Y. Wang, Y. M. Lu, B. X. Gao, S. M. Wang, J. Q. Ding, L. X. Wang, X. B. Jing and F. S. Wang, *ACS Appl. Mater. Interfaces*, 2016, **8**, 29600-29607.
4. Y. F. Gong, X. K. Fu, S. P. Zhang and Q. L. Jiang, *Chin. J. Polym. Sci.*, 2008, **26**, 91-97.
5. L. P. Hammett, *J. Am. Chem. Soc.*, 1937, **59**, 96-103.
6. F. Wu, J. L. Liu, G. Wang, Q. L. Song and L. N. Zhu, *Chem. Eur. J.*, 2016, **22**, 16636-16641.
7. X. C. Wang, L. Zhao, S. Y. Shao, J. Q. Ding, L. X. Wang, X. B. Jing and F. S. Wang, *Polym. Chem.*, 2014, **5**, 6444-6451.
8. M. Sang, S. Z. Cao, W. Y. Lai and W. Huang, *Acta Chim. Sinica*, 2015, **73**, 770-782.
9. S. K. Lee, W. H. Lee, J. M. Cho, S. J. Park, J. U. Park, W. S. Shin, J. C. Lee, I. N. Kang and S. J. Moon, *Macromolecules*, 2011, **44**, 5994-6001.
10. Y. Huang, M. Q. Zhang, L. Ye, X. Guo, C. C. Han, Y. F. Li and J. H. Hou, *J. Mater. Chem.*, 2012, **22**, 5700-5705.
11. M. J. Zhang, X. Guo, W. Ma, S. Q. Zhang, L. J. Huo, H. Ade and J. H. Hou, *Adv. Mater.*, 2014, **26**, 2089-2095.
12. M. A. Baldo, D. F. O'Brien, Y. You, A. Shoustikov, S. Sibley, M. E. Thompson and S. R. Forrest, *Nature*, 1998, **395**, 151-154.
13. S. Lamansky, P. Djurovich, D. Murphy, F. Abdel-Razzaq, H. E. Lee, C. Adachi, P. E. Burrows, S. R. Forrest and M. E. Thompson, *J. Am. Chem. Soc.*, 2001, **123**, 4304-4312.
14. Y. You and S. Y. Park, *J. Am. Chem. Soc.*, 2005, **127**, 12438-12439.
15. J. Li, P. I. Djurovich, B. D. Alleyne, M. Yousufuddin, N. N. Ho, J. C. Thomas, J. C. Peters, R. Bau and M. E. Thompson, *Inorg. Chem.*, 2005, **44**, 1713-1727.
16. Y. Chi and P. T. Chou, *Chem. Soc. Rev.*, 2010, **39**, 638-655.
17. X. L. Yang, X. B. Xu and G. J. Zhou, *J. Mater. Chem. C*, 2015, **3**, 913-944.
18. S. M. Wang, B. H. Zhang, X. D. Wang, J. Q. Ding, Z. Y. Xie and L. X. Wang, *Adv. Opt. Mater.*, 2015, **3**, 1349-1354.
19. Y. Wang, S. M. Wang, J. Q. Ding, L. X. Wang, X. B. Jing and F. S. Wang, *Chem. Commun.*, 2016, **53**, 180-183.
20. J. Q. Ding, J. H. Lu, Y. X. Cheng, Z. Y. Xie, L. X. Wang, X. B. Jing and F. S. Wang, *J. Organomet. Chem.*, 2009, **694**, 2700-2704.
21. C. Y. Kuei, W. L. Tsai, B. H. Tong, M. Jiao, W. K. Lee, Y. Chi, C. C. Wu, S. H. Liu, G. H. Lee and P. T. Chou, *Adv. Mater.*, 2016, **28**, 2795-2800.
22. P. Tao, W. L. Li, J. Zhang, S. Guo, Q. Zhao, H. Wang, B. Wei, S. J. Liu, X. H. Zhou, Q. Yu, B. S. Xu and W. Huang, *Adv. Funct. Mater.*, 2016, **26**, 881-894.
23. G. Sarada, W. Cho, A. Maheshwaran, V. G. Sree, H. Y. Park, Y. S. Gal, M. Song and S. H. Jin, *Adv. Funct. Mater.*, 2017, **27**, 1701002.

24. X. Yang, G. Zhou and W.-Y. Wong, *Chem. Soc. Rev.*, 2015, **44**, 8484-8575.
25. B. Liu, F. Dang, Z. Feng, Z. Tian, J. Zhao, Y. Wu, X. Yang, G. Zhou, Z. Wu and W.-Y. Wong, *J. Mater. Chem. C*, 2017, **5**, 7871-7883.
26. X. Yang, Z. Feng, J. Zhao, J.-S. Dang, B. Liu, K. Zhang and G. Zhou, *ACS Appl. Mater. Interfaces*, 2016, **8**, 33874-33887.
27. W.-Y. Wong and C.-L. Ho, *J. Mater. Chem.*, 2009, **19**, 4457-4482.
28. W.-Y. Wong and C.-L. Ho, *Coord. Chem. Rev.*, 2009, **253**, 1709-1758.
29. G. Tan, S. Chen, C.-H. Siu, A. Langlois, Y. Qiu, H. Fan, C.-L. Ho, P. D. Harvey, Y. H. Lo, L. Liu and W.-Y. Wong, *J. Mater. Chem. C*, 2016, **4**, 6016-6026.
30. S. Okada, K. Okinaka, H. Iwawaki, M. Furugori, M. Hashimoto, T. Mukaide, J. Kamatani, S. Igawa, A. Tsuboyama, T. Takiguchi and K. Ueno, *Dalton Trans.*, 2005, **0**, 1583-1590.
31. J. H. Seo, S. C. Lee, Y.K. Kim, Y. S. Kim *J. Nanosci. Nanotechnol.*, 2009, **9**, 7048-7051.
32. Y. Hisamatsu and S. Aoki, *Eur. J. Inorg. Chem.*, 2011, **2011**, 5360-5369.
33. Y. Jiao, M. Li, N. Wang, T. Lu, L. Zhou, Y. Huang, Z. Y. Lu, D. B. Luo and X. M. Pu, *J. Mater. Chem. C*, 2016, **4**, 4269-4277.
34. Z. M. Yan, Y. P. Wang, J. X. Wang, Y. Wang, J. Q. Ding, L. X. Wang, *J. Mater. Chem. C*, 2017, **5**, 10122-10125.
35. T. Sajoto, P. I. Djurovich, A. B. Tamayo, J. Oxgaard, W. A. Goddard and M. E. Thompson, *J. Am. Chem. Soc.*, 2009, **131**, 9813-9822.
36. S. Lamansky, P. Djurovich, D. Murphy, F. Abdel-Razzaq, R. Kwong, I. Tsyba, M. Bortz, B. Mui, R. Bau and M. E. Thompson, *Inorg. Chem.*, 2001, **40**, 1704-1711.
37. H. Yersin, A. F. Rausch, R. Czerwieniec, T. Hofbeck and T. Fischer, *Coord. Chem. Rev.*, 2011, **255**, 2622-2652.
38. H. Sasabe, H. Nakanishi, Y. Watanabe, S. Yano, M. Hirasawa, Y. J. Pu and J. Kido, *Adv. Funct. Mater.*, 2013, **23**, 5550-5555.
39. G. P. Tan, S. M. Chen, N. Sun, Y. H. Li, D. Fortin, W.Y. Wong, H. S. Kwok, D. G. Ma, H. B. Wu, L. X. Wang and P. D. Harvey, *J. Mater. Chem. C*, 2013, **1**, 808-821.
40. K. H. Kim, C. K. Moon, J. H. Lee, S. Y. Kim and J. J. Kim, *Adv. Mater.*, 2014, **26**, 3844-3847.
41. S. Lee, H. Shin and J. J. Kim, *Adv. Mater.*, 2014, **26**, 5864-5868.
42. H. U. Kim, J. H. Jang, W. Song, B. J. Jung, J. Y. Lee and D.-H. Hwang, *J. Mater. Chem. C*, 2015, **3**, 12107-12115.
43. B. Liu, J. W. Zhao, C. Y. Luo, F. Lu, S. Tao and Q. X. Tong, *J. Mater. Chem. C*, 2016, **4**, 2003-2010.

Graphic Abstract



Highly efficient green- and orange-emitting PhOLEDs have been successfully realized via a simple methoxyl modification in furo[3,2-c]pyridine based Ir complexes.